

Article

Influenza A Virus Exacerbates Group A Streptococcus Infection and Thwarts Anti-Bacterial Inflammatory Responses in Murine Macrophages

Johann Aleith ^{1,*} , Maria Brendel ¹, Erik Weipert ¹, Michael Müller ¹, Daniel Schultz ², Ko-Infekt Study Group ^{2,3,4,†} and Brigitte Müller-Hilke ¹ 

¹ Core Facility for Cell Sorting and Cell Analysis, Rostock University Medical Center, 18057 Rostock, Germany

² Institute of Biochemistry, University of Greifswald, 17489 Greifswald, Germany

³ Institute of Immunology, Friedrich-Loeffler-Institut, 17493 Greifswald-Insel Riems, Germany

⁴ Institute of Medical Microbiology, Virology and Hygiene, Rostock University Medical Center, 18057 Rostock, Germany

* Correspondence: johann.aleith@med.uni-rostock.de; Tel.: +49-381-494-5881

† Ko-Infekt Study Group: Karen Methling, Michael Lalk, Ulrike Blohm, Alexander Schäfer, Bernd Kreikemeyer.

Abstract: Seasonal influenza epidemics pose a considerable hazard for global health. In the past decades, accumulating evidence revealed that influenza A virus (IAV) renders the host vulnerable to bacterial superinfections which in turn are a major cause for morbidity and mortality. However, whether the impact of influenza on anti-bacterial innate immunity is restricted to the vicinity of the lung or systemically extends to remote sites is underexplored. We therefore sought to investigate intranasal infection of adult C57BL/6J mice with IAV H1N1 in combination with bacteremia elicited by intravenous application of Group A Streptococcus (GAS). Co-infection in vivo was supplemented in vitro by challenging murine bone marrow derived macrophages and exploring gene expression and cytokine secretion. Our results show that viral infection of mice caused mild disease and induced the depletion of CCL2 in the periphery. Influenza preceding GAS infection promoted the occurrence of paw edemas and was accompanied by exacerbated disease scores. In vitro co-infection of macrophages led to significantly elevated expression of TLR2 and CD80 compared to bacterial mono-infection, whereas CD163 and CD206 were downregulated. The GAS-inducible upregulation of inflammatory genes, such as *Nos2*, as well as the secretion of TNF α and IL-1 β were notably reduced or even abrogated following co-infection. Our results indicate that IAV primes an innate immune layout that is inadequately equipped for bacterial clearance.

Keywords: influenza A virus; Group A Streptococcus; co-infection; inflammation; sepsis; macrophage; innate immunity



Citation: Aleith, J.; Brendel, M.; Weipert, E.; Müller, M.; Schultz, D.; Ko-Infekt Study Group; Müller-Hilke, B. Influenza A Virus Exacerbates Group A Streptococcus Infection and Thwarts Anti-Bacterial Inflammatory Responses in Murine Macrophages. *Pathogens* **2022**, *11*, 1320. <https://doi.org/10.3390/pathogens11111320>

Academic Editors: Getahun Abate and Lawrence S. Young

Received: 30 September 2022

Accepted: 8 November 2022

Published: 10 November 2022

Publisher's Note: MDPI stays neutral with regard to jurisdictional claims in published maps and institutional affiliations.



Copyright: © 2022 by the authors. Licensee MDPI, Basel, Switzerland. This article is an open access article distributed under the terms and conditions of the Creative Commons Attribution (CC BY) license (<https://creativecommons.org/licenses/by/4.0/>).

1. Introduction

Seasonal influenza is a major cause of respiratory disease that affects 5–10% of the global population annually with an estimated death toll of up to 500,000 [1,2]. The segmented genome of influenza A virus (IAV) combined with an error-prone RNA polymerase enables the periodical emergence of new strains with elevated pandemic capacities, which annually challenge humankind yet are devoid of adequate adaptive immunity [3,4]. The most prominent paradigm for the dramatic consequences of an influenza pandemic is the 1918/1919 flu that caused roughly 50 Million casualties [5]. Notably, the vast majority of fatal cases were attributed to secondary bacterial infections predominantly caused by pneumococci and hemolytic streptococci [6,7]. Along these lines, excess morbidity due to bacterial superinfection with the nasopharyngeal colonizers *S. pneumoniae*, *S. aureus* and *S. pyogenes* (Group A Streptococcus, GAS) was confirmed for the most recent influenza pandemic in 2009 [8]. As of yet, there is neither a licensed vaccine against *S. aureus* nor

against *S. pyogenes* that would help contain invasive infections with these pathogens during future influenza pandemics [9–11].

Several modes by which an immune response against IAV supports viral clearance yet fails to oppose bacterial pathogens have been suggested [1]. For instance, Okamoto et al. demonstrated that IAV infection led to the presentation of hemagglutinin (HA) by epithelial cells, which is utilized by GAS to breach cellular barriers [12,13]. Other groups reported that HA, among other viral proteins, caused the exposure of receptors that act as adhesins for bacterial attachment and invasion [14–16]. Others showed that viral infection caused damage of the respiratory epithelium, which expedited the initial bacterial adherence [6,17,18]. Moreover, experimental data indicated that IAV paves the way for the dissemination of opportunistic bacterial pathogens by impacting the innate immune response, which is critical for bacterial containment [19,20]. In fact, the virus was shown to induce an increased secretion of anti-inflammatory interleukin (IL-)10 as well as inflammatory type I and type II interferons (IFNs), which were associated with both impaired phagocytic activity by pulmonary immune cells and diminished production of chemokines [14,19,21–24].

Together, these data illustrate some aspects of post-influenza pneumonia and the interplay of viral and bacterial pneumopathogens in life-threatening infections. While the aforementioned studies focused on bacterial superinfections of the respiratory tract, we were intrigued that seasonal or pandemic influenza outbreaks seem to coincide with a broad spectrum of invasive GAS-associated infectious diseases like necrotizing fasciitis, pneumonia and bacteremia [8,25–30]. We therefore asked whether pulmonary IAV can also alter systemic innate immunity and facilitate secondary bacterial insults at remote sites. We were particularly interested in the impact IAV exerts on the response of macrophages (immune cells that are indispensable for initial anti-streptococcal resistance [19,31,32]). We established co-infection models that combined respiratory IAV infection with GAS bacteremia *in vivo*, and investigated primary macrophages for their potential to respond to both pathogens simultaneously *in vitro*.

2. Materials and Methods

2.1. Pathogens

Pandemic influenza A virus (IAV) A/Germany-BY/74/2009 (H1N1pdm09) propagation and titer determination was performed as previously described [33]. In brief, IAV was replicated in Mardin–Darby canine kidney II (MDCKII) cells using a minimal essential medium supplemented with 0.2% bovine serum albumin and 2 µg/mL N-Tosyl-L-phenylalanin-chlormethylketon (Sigma, Kawasaki-shi, Japan). For the determination of the tissue culture infectious dose 50 (TCID₅₀), virus suspensions were serially diluted and applied to MDCKII cultures. Cells were then incubated for three days at 37 °C and 5% CO₂, followed by examination of cytopathogenicity.

Streptococcus pyogenes (Group A Streptococcus, GAS) strain AP1 of the *emm1* (M1) serotype was originally acquired from the World Health Organization Collaborating Center for Reference and Research on Streptococci (Prague, Czech Republic). Bacteria were thawed onto Columbia agar plates containing 5% sheep blood (Becton Dickinson, Franklin Lakes, NJ, USA) and were cultured overnight, followed by storage at 4 °C for up to three weeks. Colonies were picked from the plate, suspended into Todd-Hewitt broth (THB, Becton Dickinson) and cultured overnight at 37 °C and 5% CO₂. The suspension was diluted 20-fold in THB and bacteria were incubated until an exponential phase of growth was reached. Subsequently, bacteria were washed thrice with PBS (Thermo Fisher, Waltham, MA, USA) prior to their application in mice and *in vitro* infection models, respectively. The determination of colony forming units (CFU) was performed the following day by counting the serially diluted suspensions.

2.2. Animals

C57BL/6J mice were initially purchased from Charles River. Mice were bred in the animal core facility under specific germ-free conditions. Animals were transferred to individually ventilated cages prior to infection experiments and were housed at a 12-h light/dark cycle, an ambient temperature of 22 ± 2 °C and $50 \pm 20\%$ humidity. Food and water were provided ad libitum. Animal experiments were reviewed and approved by the ethics committee of the State Department for Agriculture, Food Safety and Fishery in Mecklenburg–Western Pomerania under the file reference number 7221.3-1-017/19.

2.3. In Vivo Infection Models and Clinical Scoring

For the induction of viral infections, 20 μL of a suspension containing 1.5×10^5 TCID₅₀ IAV were applied to both nostrils of 20- to 22-week-old male mice under anesthesia by isoflurane inhalation. This volume was chosen in order to guarantee an infection of both the upper and lower respiratory tracts [34]. Applying the same volume of PBS only served as the negative (healthy) control. Mice were subsequently monitored daily for 16 days for alterations in body weight relative to the day of infection (day 0). On days 2, 4 and 7, a maximum of 80 μL of anti-coagulated blood was drawn by saphenous venipuncture using a 25G needle followed by centrifugation and collection of plasma. On day 16, mice were anesthetized with 75 mg of Ketamine (Pharmanovo) and 5 mg Xylazin (Bayer) per kg bodyweight. Subsequently, mice were exsanguinated by cardiac puncture. Mice were then sacrificed by cervical dislocation and lungs were excised, snap frozen and stored at -80 °C for later analyses.

In order to induce bacteremia, GAS was diluted in PBS and 1×10^5 CFU were applied in a 100 μL volume by injection into the lateral tail vein. Intravenous injection of PBS served as a control. For co-infection, IAV was applied as described above either two days prior or subsequent to bacterial infection. Mice were given tramadol (Ratiopharm) in drinking water for analgesia. Animals were monitored following bacterial infection for a maximum of 14 days or until humane endpoints were reached. Sepsis severity was assessed by a scoring system that incorporated the assessment of macroscopic signs of burden as previously described [35,36]. In brief, the scores of four categories were added together to provide an estimate for overall sepsis activity: (i) weight loss of $\geq 5\%$ (Score 5), $\geq 10\%$ (Score 10), $\geq 20\%$ (Score 20, humane endpoint); (ii) appearance deviations, such as piloerection (Score 5), high myotonicity or scruffy orifices (Score 10), convulsions or paralysis (Score 20, humane endpoint); (iii) impairment of consciousness, such as suppressed activity or limited reaction to stimuli (Score 5), self-isolation or lethargy (Score 10), perpetual pain vocalization or apathy (Score 20, humane endpoint); and iv) signs of impaired respiratory quality or inflammation such as edemas on small body areas (Score 5), disseminated edemas or labored breathing (Score 10), open wounds or gasping (Score 20, humane endpoint).

Mice were sacrificed as described above upon reaching the end of the observation period, at any humane endpoint or when reaching an overall sepsis score of ≥ 20 . Cardiac blood samples were plated on blood agar and medial arthrotomy on both knee joints was performed under a stereo microscope followed by plating of the synovial fluid on blood agar. Agar plates were subsequently incubated overnight and examined for the presence of β -hemolytic bacteria. Hind paws were extracted, snap frozen and stored at -80 °C for the analysis of eicosanoids.

2.4. Eicosanoid Extraction and Analysis

Lipidomic analyses were performed as previously described [35]. In brief, paw samples were chilled in liquid nitrogen, pulverized and 50 mg of the resulting powder was immersed in 500 μL cold methanol containing 0.1% butylated hydroxytoluene and 500 μL ice cold water. 100 μL deuterated internal standards containing 12-HETE-d₈, 13-HODE-d₄, PGE₂-d₄ and Resolvin D1-d₅ (each 100 ng/mL, Cayman Chemicals, Ann Arbor, MI, USA) were subsequently added followed by an additional lysis step with matrix B at 6 m/s for 45 s on a FastPrep (MP Biomedicals, Santa Ana, CA, USA). Following this, 300 μL sodium

acetate (1 M) was added on ice and 10 M acetic acid was added until pH 6 was reached. Solid phase extraction was performed on methanol and sodium acetate conditioned Bond Elut Certify II cartridges (Agilent). After loading the samples, cartridges were washed with 50% methanol. Elution of eicosanoids was carried out by the addition of hexane/ethyl acetate (75/25) containing 1% acetic acid.

For measurements, paw extracts were dried under nitrogen flow using a TurboVap (Biotage, Uppsala, Sweden) and reconstituted in 70 μ L 25% acetonitrile. Separation was done on a Gemini NX-C18 column (3 μ m, 100 \times 2 mm) utilizing an Agilent 1200 series HPLC system. Dynamics multiple reaction monitoring MS/MS was executed using a 6460 series triple quadrupole tandem mass spectrometer (Agilent) with electrospray ionization in negative mode. Calibration by internal and external standards was performed as previously described [35]. Agilent Mass Hunter Qualitative Analysis software and Agilent Mass Hunter Quantitative Analysis software (both version B.07.00) were used for MS data analysis. Quantities of individual eicosanoids were standardized to a mean of 0 and a standard deviation of 1 for data visualization.

2.5. Isolation of RNA and DNA from Lung Samples

Lung samples were submerged in liquid nitrogen, slightly fragmented and weighed. Sixty to one hundred twenty milligrams were transferred to lysis tubes containing bashing beads (Zymo Research, Irvine, CA, USA) and 1 mL TRIzol (Thermo Fisher, Waltham, MA, USA). Lung fragments were subsequently homogenized at 4000 rpm for 4 \times 20 s using a FastPrep. Samples were then centrifuged at 10,000 \times g for 7 min at 4 $^{\circ}$ C and transferred into new tubes. Apart from centrifugation at 4 $^{\circ}$ C, the following steps were conducted at room temperature. After resting for 5 min, 200 μ L chloroform (Sigma) was added and samples were extracted for 3 min. Subsequently, samples were centrifuged for 15 min at 12,000 \times g. The RNA-enriched upper phase was mixed with 500 μ L 2-propanol, incubated for 10 min and centrifuged at 12,000 \times g for 10 min. RNA pellets were suspended in 75% Ethanol followed by centrifugation at 7500 \times g for 5 min. Supernatants were subsequently discarded, pellets were dried and dissolved in 40 μ L RNase-free water by incubation at 60 $^{\circ}$ C for 15 min. RNA contents were then determined photometrically on a NanoDrop (Thermo Fisher). DNA was isolated by precipitation of the appropriate phase upon the addition of 300 μ L ethanol, incubation for 3 min and centrifugation for 5 min at 2000 \times g. The resulting pellet was then washed twice by 30 min incubation with 0.1 M sodium citrate (pH 8.5) in 10% ethanol. DNA samples were subsequently suspended in 75% ethanol and incubated for 20 min. After centrifugation, supernatants were discarded, pellets were dried and then dissolved by incubation in 8 mM NaOH for 10 min. DNA contents were determined fluorometrically using the Qubit 1X dsDNA Assay Kit to the manufacturer's instructions (Thermo Fisher, Waltham, MA, USA).

2.6. Lung Pathogen Genetic Material and Gene Expression

Primer pairs were designed for the detection of IAV H1N1 matrix protein, nucleoprotein and hemagglutinin in murine lung RNA extracts according to the strain specific sequences found at <https://www.fludb.org/brc/fluStrainDetails.spg?strainName=A%2FGermany-BY%2F74%2F2009%28H1N1%29&decorator=influenza> (accessed on 20 September 2022) (Supplementary Table S1). For this, RNA was isolated as described above and 500 ng were reverse transcribed using the High Capacity cDNA Reverse Transcription Kit (Thermo Fisher, Waltham, MA, USA) according to the manufacturer's instructions. Twenty-five nanograms of the resulting cDNA together with 500 nM of the primer pairs were submitted to qPCR using the PowerUP SYBR Green Mastermix (Thermo Fisher). The amplification reaction was monitored on the ViiA 7 Real-Time PCR System running on the QuantStudio Real Time PCR Software V1.3 (Thermo Fisher). The size of the respective amplicons was confirmed by 2% agarose gel and ethidium bromide staining. Primer pairs for the detection of GAS strain AP1 specific genomic DNA were designed according to sequence information found at <https://www.ncbi.nlm.nih.gov/nuccore/CP007537?report=genbank> (accessed on 20 September 2022) (Supplementary Table S2). A total of 20 ng DNA from lung extracts were used together with 500 nM of the primer pairs for qPCR,

as described above, followed by confirmation of amplicon sizes on agarose gels. Gene expression analyses were performed on 25 ng cDNA that was obtained from reverse-transcribed lung RNA. For qPCR analysis, TaqMan primer pairs and probes (Thermo Fisher, Waltham, MA, USA) were used for *Ccl2* (assay ID: Mm00441242_m1) and *Ifnb1* (Mm00439552_s1) utilizing *Gapdh* (Mm05724508_g1) as a reference gene. All reactions were amplified using the TaqMan Gene Expression Master Mix (Thermo Fisher).

2.7. Bone Marrow Derived Macrophage Infection Model

The C57BL/6J mice used for bone marrow isolation had a median age of 10 weeks (range 7–42 weeks) and 30% were female. Bone marrow was obtained from long bones by centrifugation, as previously described [37]. The resulting pellet was subsequently suspended in Dulbecco's Modified Eagle's Medium (DMEM) supplemented with 10% fetal calf serum (FCS), 5 IE/mL Penicillin, 5 µg/mL Streptomycin, 2 mM L-Glutamine (Thermo Fisher, Waltham, MA, USA), 10 mM HEPES and 1 mM sodium pyruvate (PAN Biotech, Aidenbach, Germany). After determination of vital cells using a hemocytometer and trypan blue (Thermo Fisher), cells were seeded into 6-well culture plates (Greiner) at a density of 3×10^5 cells per cm^2 in 2–5 mL supplemented DMEM. The differentiation to macrophages was initiated at day 0 by the addition of 20 ng/mL macrophage colony-stimulating factor (M-CSF, R&D Systems, Minneapolis, MN, USA). Cells were cultured afterwards at 37 °C and 5% CO₂ for 7 days including the replacement of supplemented DMEM and replenishment of M-CSF at days 1 and 4. For viral infection (day 7, t₀), supplemented DMEM was refreshed and 4×10^5 TCID₅₀ IAV were added. Following this, infected or uninfected macrophages were incubated for 48 h upon which the cells were either collected for downstream analyses or submitted to bacterial (super-)infection (day 9). In the case of the latter, supplemented DMEM was removed, the cells were washed thrice with PBS and Minimal Essential Medium α containing additional nucleosides and 10% FCS (Thermo Fisher, Waltham, MA, USA) was added; GAS was then applied at 4.5×10^6 CFU. Subsequently, macrophages were incubated for 6 h followed by sample collection.

2.8. Single Cell Analysis by Flow Cytometry

Gentle detachment of macrophages from culture plates was carried out by washing with PBS and subsequently incubating with 5 mL PBS containing 10 mM EDTA for 10 min. Culture plates were tapped multiple times and suspensions were collected afterwards. For increased yields, 0.7 mL accutase (Pan Biotech) was added for 10–15 min followed by alternately tapping and pipetting. Subsequently, another 0.7 mL accutase were added for an additional 10–15 min, tapping and pipetting were repeated and suspensions were collected and pooled with the PBS/EDTA fraction. Finally, 1 mL supplemented DMEM was added and the remaining cells were obtained using a cell scraper (Sarstedt, Mawson Lakes, Australian). Suspensions were centrifuged at $400 \times g$ and 4 °C for 5 min and cells were suspended in autoMACS Running Buffer (RB, Miltenyi Biotec, Bergisch Gladbach, Germany) followed by counting. Antibody binding to CD16 and CD32 was prevented by the incubation of macrophages with 0.5 µg Trustain FcX (Biolegend, San Diego, CA, USA) in RB supplemented with 10% FCS for 10 min on ice. Subsequently, an antibody mixture containing 0.13 µg (anti-)F4/80:FITC (clone BM8), 0.5 µg CD163:APC (S150491), 0.25 µg CD206:BV605 (C068C2), 0.25 µg CD80:BV421 (16-10A1, Biolegend), 0.22 µg CD86:APC/Vio770 (PO3.3), 4.5 µL TLR2:PE (REA109) and 0.15 µg MHCII:PerCP/Vio770 (REA813, Miltenyi Biotec) was added and incubated for 20 min on ice in the dark. Cells were washed afterwards, suspended in RB and 7-Aminoactinomycin (7-AAD, Biolegend) was added at a concentration of 1.25 µg/mL for at least 5 min prior to measurement.

Data acquisition was performed on the Aurora spectral flow cytometer running on the SpectroFlo software v2.2.0.3 (Cytek Biosciences, Fremont, CA, USA). Data analysis was conducted using the FlowJo software v10.7.1. Supplementary Figure S1 illustrates the gating strategy. Live macrophages were identified as 7-AAD⁻F4/80⁺ singlets. This population was used for the subsequent determination of expression levels based on me-

dian fluorescence intensity (MFI) values and as a parent for measuring the proportions of subpopulations expressing different combinations of the above-listed surface antigens. For dimension reduction, 10,000 macrophage events were down-sampled, concatenated and submitted to the algorithm t-distributed stochastic neighbor embedding (t-SNE) using an automated learning configuration (opt-SNE combined with the exact KNN algorithm and the Barnes-Hut gradient algorithm) with a perplexity of 50 and a maximum of 1000 iterations [38]. Unsupervised clustering of subpopulations expressing any combinations of the analyzed surface proteins was conducted by FlowSOM [39].

2.9. Macrophage Gene Expression

After aspirating cell culture supernatants, 700 μ L of a chaotropic agent solution (Qiagen) was added to individual wells, and cells were lysed by scraping and vigorous shaking. RNA was subsequently isolated using the RNeasy Plus Mini Kit (Qiagen) after the manufacturer's instructions. Quantification of RNA contents were determined photometrically and 200 ng RNA was submitted to reverse transcription as described above. Amplification of cDNA was then performed by TaqMan Gene Expression Master Mix, primer pairs and probes for the relative quantification of *Ccl2*, *Cxcl2* (assay ID: Mm00436450_m1), *Ifnb1*, *Il1b* (Mm00434228_m1), *Il6* (Mm00446190_m1), *Il10* (Mm00439614_m1), *Mgl2* (Mm00460844_m1), *Nos2* (Mm00440502_m1), *Tgfb1* (Mm01178820_m1) and *Tnf* (Mm00443258_m1) using *Gapdh* as a reference gene. Polymerase chain reactions were performed on the ViiA 7 System. In detail, samples were first incubated for 2 min at 50 °C followed by 10 min at 95 °C for polymerase activation. Subsequently, 40 automated cycles of PCR were performed that incorporated denaturation at 95 °C for 15 sec and annealing and elongation at 60 °C for 1 min. After each cycle, the fluorescein amidite fluorescence signal was measured. Ct values were obtained when fluorescence intensities reached data-dependent and automatically defined thresholds. Quantification of gene expression was then performed by the $2^{-\Delta\Delta C_t}$ Method that incorporated normalization of the target gene Ct values to the reference gene (ΔC_t) as well the difference between ΔC_t values from uninfected and infected cells ($\Delta\Delta C_t$).

2.10. Cytokine Analysis

Cytokine concentration in mouse plasma samples were quantified by a 3-plex LEGENDplex assay (Biolegend) that contained capture beads and detection antibodies for CCL2 (monocyte chemoattractant protein-1, MCP1), Interferon (IFN) γ and tumor necrosis factor (TNF) α . For the quantification of CCL2, Interleukin (IL-1) β , IL-6, IL-10 and TNF α in cell culture supernatants, a 5-plex LEGENDplex assay was used following the manufacturer's guidelines. Data acquisition was performed on the Cytex Aurora flow cytometer. Cell culture supernatant concentrations of CXCL2 (macrophage inflammatory protein 2- α , MIP2- α) were determined by the CXCL2/MIP-2 DuoSet enzyme linked immunosorbent assay (ELISA) kit to the manufacturer's instructions (R&D Systems). Horseradish peroxidase-catalyzed color reactions were initiated by the addition of the TMB Substrate Kit (Biolegend) and quenched by 0.5 M sulfuric acid (Merck). The absorbance at 450 nm was measured on the Infinite M200 spectral photometer (Tecan).

2.11. Statistical Analysis

Data analysis and visualization were performed using RStudio v1.2.5033 that ran R v3.5.1. Normalization was either performed by division of individual values from infection groups and control groups, respectively, or by feature scaling into a 0–1 range by the formula $x'_i = (x_i - x_{\min}) / (x_{\max} - x_{\min})$. Feature scaling was used in Figure 1D,E and Figure 2G. Heatmaps and hierarchical clusters were generated with the “pheatmap” package that incorporated feature scaling by applying standardization to the formula $z_i = (x_i - \bar{x}) / \sigma$. Calibration curves were fitted and samples values were estimated by n-parameter logistic regression using the “nplr” package. Two-sided statistical tests were used for the comparisons of group medians or means. Repeated measures (body weight trajectories) were compared by one-way and two-way analyses of variance (ANOVA), respectively.

Probabilities of survival and incidences were compared by the logrank test. Bivariate interdependencies were evaluated by the Pearson product-moment correlation coefficient (r). Data sets were tested for normality by the Shapiro-Wilk test. Normal distribution of within-group raw or normalized variables was rejected when the test resulted in a p -value of < 0.05 . Depending on the outcome of this test, univariate statistical analyses on variables that were normalized to respective controls were performed by the one-sample Wilcoxon signed rank test and the one-sample t -test, respectively. Two independent samples were compared with the Mann-Whitney U test or the t -test. Comparisons of variables between multiple groups were performed with the Dunn's test and the Tukey HSD test, respectively, in combination with type I error correction using the Bonferroni-Holm method. A p -value of < 0.05 was considered statistically significant.

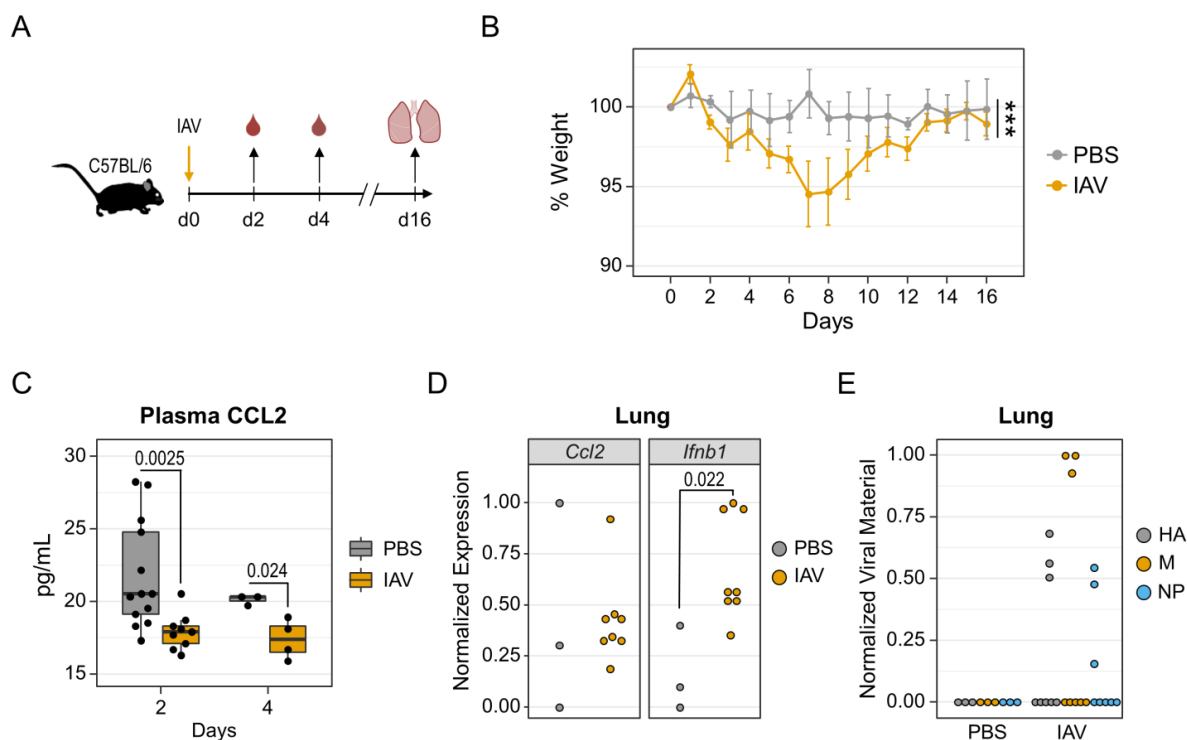


Figure 1. Influenza A virus infection induced minor weight loss and inhibited the production of CCL2. (A) Experimental Design. Mice were intranasally infected with influenza A virus (IAV, $n = 8$). PBS was administered as a control ($n = 3$). Blood samples were drawn on days 2 and 4 following infection. Lungs were excised at day 16. (B) Mean weight changes relative to day 0. Weight loss was confirmed by one-way ANOVA ($p < 0.0001$) in the IAV group and by two-way ANOVA ($*** p < 0.001$) comparing the IAV group to PBS controls. Error bars depict the SEM. (C) Boxplots display CCL2 concentrations in plasma samples from uninfected controls ($n = 13$) and IAV infected mice ($n = 9$). The differences in samples size between days 2 and 4 are due to the fact that some animals were later subjected to the bacterial and co-infection experiments that are shown in Figure 2. Day 2 and Day 4 p -values result from Mann-Whitney U test and t -test, respectively. (D) Dotplots show normalized mRNA expression of *Ccl2* and *Ifnb1* in lung homogenates based on ΔCt values; p -value results from t -test. (E) Normalized viral genetic material based on reciprocal Ct values for IAV specific genes in day 16 lung homogenates. HA: hemagglutinin, M: matrix protein, N: nucleoprotein. Zero values represent the detection limit that corresponds to Ct value greater than 40.

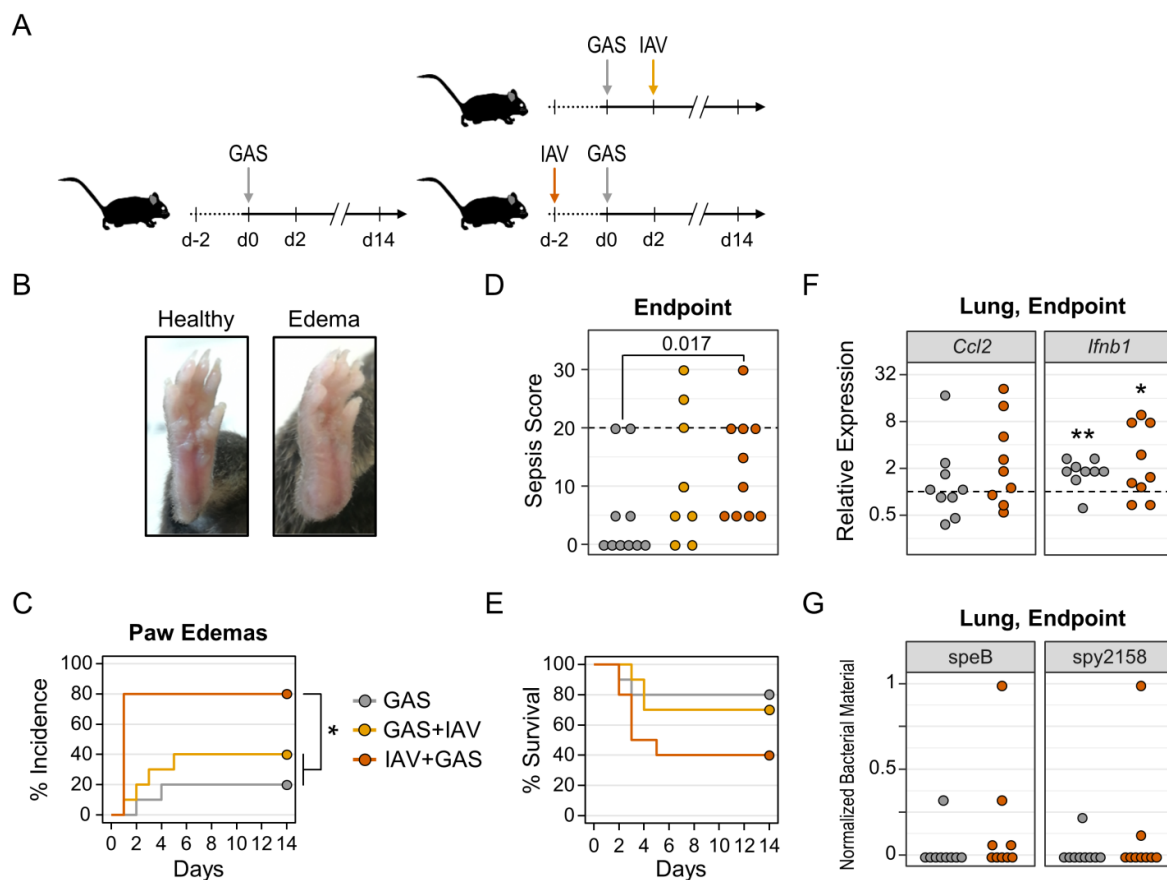


Figure 2. Preceding IAV infection promotes paw edemas and sepsis severity during co-infection. (A) Experimental design. For monocausal bacterial infection, Group A Streptococcus was administered intravenously (GAS, $n = 10$). For co-infection, mice were either infected with GAS followed by intranasal IAV administration (GAS+IAV, $n = 10$) or infected with IAV followed by infection with GAS (IAV+GAS, $n = 10$). (B) Representative photographs of a healthy paw compared to an edematous paw after IAV+GAS co-infection. (C) Kaplan–Meier curves display the incidences of paw edemas. * $p < 0.05$, log-rank test with p -value adjustment for multiple comparisons (Bonferroni–Holm method). (D) Dotplot shows sepsis scores at endpoints (day 14 or humane endpoint). p -value results from Mann–Whitney U test. The dashed line indicates the minimum score for humane endpoints. (E) Kaplan–Meier curves display survival probabilities. (F) Dotplots show endpoint bulk lung mRNA gene expressions of *Ccl2* and *Ifnb1* that were normalized to *Gapdh* and lungs from uninfected mice (dashed line) by the $2^{-\Delta\Delta C_t}$ method. * $p < 0.05$, ** $p < 0.01$, one-sample Wilcoxon signed-rank test ($\mu = 1$). (G) Normalized bacterial genetic material based on reciprocal C_t values for GAS specific genes in endpoint lung DNA extracts. Zero values represent the detection limit that corresponds to C_t value greater than 40.

3. Results

3.1. Infection with Influenza A Virus H1N1 Caused Mild Symptoms and Reduced CCL2 in the Periphery

In order to examine clinical manifestations of influenza, we used a model of intranasal infection with 2009 pandemic H1N1 IAV in adult mice (Figure 1A). Intranasal application of PBS served as a control. Mice were monitored for relative weight loss post infection as a proxy for disease severity and indeed exhibited minor reductions in body weight as early as two days after virus application (Figure 1B). This trend continued until day seven after infection and resulted in a maximum weight loss of $5.5\% \pm 2.1\%$ (mean \pm SEM). Thereafter, body weight continuously increased and returned to the starting values by day 14, which suggests robust recovery from infection. When comparing weight trajectories over the entire observation period using two-way analysis of variance (ANOVA), we

found a statistically significant difference between infected mice and uninfected controls ($p < 0.001$). In accordance with the observed mild disease courses, we did not measure quantifiable amounts of the inflammatory cytokines $\text{TNF}\alpha$ and $\text{IFN}\gamma$ in plasma samples from IAV infected animals (not shown). We did, however detect significant reductions of plasma CCL2 concentrations by 12.8% and 13.6% at days two and four after infection, respectively, relative to uninfected controls (Figure 1C). By day seven, CCL2 plasma levels equalized between both groups ($p = 0.65$, not shown). These data hint at a transiently impaired chemotaxis of innate immune cells due to IAV infection, as CCL2 is a potent attractant for monocytes [40].

In order to examine immune responses in the lower respiratory tract, we further performed gene expression analyses on whole lung homogenates that were obtained 16 days after IAV application. For this, we focused on mRNA expression levels of *Ccl2* and *Ifnb1*, as the former was altered in the periphery and the latter can be indicative of an anti-viral response. Protein data were not collected because of limited sample quantities. We found no meaningful differences in the expression of *Ccl2* between the IAV and control groups (Figure 1D, left panel), which indicates that monocyte homing to the lung was not affected in the late stages of IAV infection. Interestingly, *Ifnb1* expression was found to be significantly increased in the lungs of infected mice (Figure 1D, right panel). Given this prolonged upregulation of *Ifnb1*, we consequently utilized primer pairs for the detection of viral genes in lung samples that code for hemagglutinin, matrix protein and nucleoprotein (Supplementary Figure S2). We indeed detected IAV-specific RNA in 38% (3/8) of infected animals by quantitative PCR (Figure 1E). False positive detection of unspecific targets was ruled out by confirming the expected amplicon melting temperatures (Supplementary Figure S3). However, the quantities of all three viral genes were generally low ($C_t > 32$) and might rather indicate residual viral antigen. Interestingly, two of the three samples that were positive for viral genes were also among the samples that expressed the highest amounts of *Ifnb1*, which indicates that there is some correlation between both parameters.

In summary, we here show that an infection with IAV H1N1 in mice induced by minor clinical manifestations that were accompanied by an early and reversible reduction of plasma CCL2 levels. Our data further show that barely detectable genetic material of the virus persisted in the lungs of some animals, which was accompanied by an ongoing type I IFN production.

3.2. Group A Streptococcal Infection Was Aggravated Following Influenza A Virus Infection

As CCL2 is integral to bacterial control [24,41,42], yet is reduced during respiratory tract infection with IAV. We sought to investigate the clinical features of IAV superimposed bacteremia. To this end, we compared infection with bacteria only to co-infection models combining intranasal virus application with intravenous GAS infection in alternating succession (Figure 2A). By monitoring for macroscopic symptoms following bacterial infection, we observed the occurrence of localized paw inflammation (Figure 2B). Of note, the emergence of these edemas was accelerated and more frequent in post-influenza bacteremia (IAV+GAS) compared to bacterial infection only (GAS, $p = 0.01$) and pre-influenza bacteremia (GAS+IAV, $p = 0.045$), respectively (Figure 2C). In detail, 80% (8/10) of mice in the IAV+GAS group exhibited signs of paw inflammation already one day after bacterial infection. In contrast, the incidence of paw edemas was increased to only 40% (4/10) in the GAS+IAV group as opposed to 20% (2/10) in the GAS only group; this difference did not reach statistical significance ($p = 0.33$). In a recent study, we found that eicosanoid quantities were correlated with localized GAS induced inflammation [35]. Hence, we analyzed eicosanoids from paw extracts and found that these immunologically active lipid metabolites were upregulated in some animals irrespective of the (co-)infection regimen (Supplementary Figure S4).

Additionally, more blood smears and knee joint capsule swabs were positive for β -hemolytic bacteria in co-infected mice from the IAV+GAS group (Table 1), which suggested that preceding influenza promoted bacterial dissemination and invasion into synovial tis-

sues. By assessing macroscopic signs of burden as a proxy for sepsis severity (see Materials and Methods), we found a significantly increased median disease score when comparing post-influenza bacteremia with monocausal GAS infection (Figure 2D). Interestingly, when correlating sepsis scores with eicosanoids from paw homogenates, we found a significant relationship between the individual disease severity and the corresponding amounts of prostaglandins D₂ and E₂ as well as 5- and 12-Hydroxyeicosatetraenoic acid (Supplementary Table S3). Furthermore, elevated disease severity in the IAV+GAS group was paralleled by a reduction in survival probability to 40% compared to 80% in the GAS only group (Figure 2E). In contrast, mice from the GAS+IAV group had an only marginally decreased survival chance of 70%. However, the overall probability for a fatal outcome was, according to logrank statistics, not significantly different between groups ($p = 0.13$) and this was likely due to low sample sizes and a high degree of uncertainty.

Table 1. Frequencies of blood agar cultures from endpoint blood smears and synovial knee joint swabs positive for β -hemolytic bacteria.

Positive Cultures	GAS	GAS+IAV	IAV+GAS
blood	20% (2/10)	30% (3/10)	50% (5/10)
knee joint capsule	10% (1/10)	30% (3/10)	50% (5/10)

$p = 0.25$, Fisher's exact test.

For our further analyses, we focused on the IAV+GAS co-infection sequence because our data suggested that the clinical outcome was not different between the GAS+IAV and GAS groups. We next aimed to investigate whether post-influenza GAS infection impacted the immune activation in the lower respiratory tract. To this extent, we analyzed lung homogenates for the expression of *Ccl2* and *Ifnb1*, and compared the data from co-infected mice to GAS mono-infection or uninfected controls. We found that neither GAS nor IAV+GAS infection resulted in a meaningful alteration of the *Ccl2* expression in the lung (Figure 2F, left panel). Of note, lungs from both mono- and co-infected mice exhibited a median 2-fold upregulation of *Ifnb1* relative to lungs from uninfected animals ($p = 0.008$ for GAS and $p = 0.039$ for IAV+GAS; Figure 2F, right panel). Yet, when comparing the infection regimens with each other, we found that *Ifnb1* overexpression was comparable between both infection groups ($p = 0.93$). We were curious whether the bacteria are capable of disseminating from the blood into the lower respiratory tract and therefore analyzed lung homogenates for the presence of GAS specific genes using quantitative PCR (Supplementary Figure S5). Indeed, we detected genomic *speB* in four out of nine lungs from the IAV+GAS group whereas only one out of nine lungs from the GAS group was positive for this bacterial gene (Figure 2G, left panel). However, when analyzing for *spy2158*, only two lung extracts from the IAV+GAS group were positive (Figure 2G, right panel). Specific amplification was again confirmed by melting curves (Supplementary Figure S6). As whole lungs were submitted to chaotropic agent assisted homogenization and PCR analysis, we were not able to confirm whether there were any vital bacteria present in these samples.

Collectively, our in vivo data demonstrated that a preceding IAV infection of the respiratory tract aggravated intravenous GAS infection by promoting localized inflammation and a dysregulated host response, as shown by elevated sepsis scores. In contrast, application of the virus following an already established bacteremia did not influence on disease progression and outcome.

3.3. Preceding Influenza A Virus Infection Impacted on the Group A *Streptococcus* Induced Diversification of Macrophage Surface Expression Profiles

As our in vivo co-infection model implicated a preceding IAV infection to cause impaired control of the bacterial challenge following a superimposed GAS infection, we sought to explore any modification of anti-bacterial innate immunity. Macrophages are considered as first line defense immune cells that are substantial to contain pathogens in early phases of infection [43]. These cells take part in numerous bacterial infectious

diseases and are especially crucial for a competent innate immune response during invasive GAS infection [31,44–46]. Hence, we chose in vitro (co-)infection models of primary murine macrophages in order to investigate whether IAV influences the GAS-induced immune landscape. In detail, murine macrophages were differentiated from bone marrow cells by M-CSF stimulation and were subsequently infected with IAV, GAS or IAV and GAS (Figure 3A). We then analyzed the expression patterns of immunologically relevant surface antigens by flow cytometry. In order to gain insight into differentially expressed macrophage markers, we performed dimension reductions on our multiparametric data sets by t-distributed stochastic neighbor embedding (t-SNE). Figure 3B demonstrates the topological distribution of surface marker expression levels' distinct allocations of cells that were obtained from the different infection models. For instance, macrophage subsets overexpressing CD80 and CD86 were seemingly enriched in IAV+GAS co-infected cultures, whereas mono-infection with GAS resulted in the accumulation of CD206 overexpressing macrophages. Unsupervised clustering of macrophage populations on the basis of their respective expression patterns by flowSOM further indicated that co-infection triggered a different response than viral or bacterial mono-infections (Supplementary Figure S7).

In an effort to obtain a more detailed picture of IAV- and GAS-induced immune responses, we next focused on the individual expressions of macrophage surface antigens. Given the inter-experimental variance of macrophage cultures, median fluorescence intensities (MFI) of (co)-infected cells were normalized to their corresponding uninfected controls that were acquired from the same donor animal (Supplementary Figure S8). Notably, expression patterns were similar within each group, which resulted in a robust hierarchical clustering for IAV, GAS and IAV+GAS infected macrophages (Figure 3C). In detail, apart from a significant upregulation of CD163 compared to both bacterial infection and co-infection, IAV had hardly any impact on the expression of the investigated surface proteins (Figure 3C,D). Conversely, GAS infection induced the overexpression of TLR2, which was even amplified following co-infection (Figure 3D). Both the applications of GAS and IAV+GAS comparably prompted an elevated production of MHCII. Although not statistically significant, GAS infection led to a slight downregulation of CD80, which was reversed to an upregulated expression in the IAV+GAS group. Similarly, co-infection triggered a minor overexpression of CD86 that was short of reaching statistical significance due to a high within-group variance ($p = 0.067$, compared to uninfected). The downregulation of CD163, as well as the attenuation of the GAS-induced CD206 upregulation in the IAV+GAS group, further supports the notion that a preceding IAV infection led to a distinct immune response in macrophages during co-infection (Figure 3D).

As a result of differentially affected expression landscapes, the proportions of distinctive macrophage subpopulations shifted depending on the infection regimen (Figure 3E). We found a minor depletion of CD80⁺CD86⁺ cells following GAS infection ($p = 0.1$), whereas co-infection caused a significantly increased proportion of this population when compared to uninfected controls (Figure 3F). Both bacterial mono-infection and co-infection induced an enrichment of MHCII⁺ macrophages, which suggests a retained ability of these immune cells to inform and coordinate an adaptive immune response. In accordance with the altered expression profiles shown in Figure 3D, the proportions of CD163⁺ and CD206⁺ cells, respectively, were decreased upon co-infection relative to GAS infection only (Figure 3F).

Collectively, our data on the diversification of surface antigen expression demonstrated that the immune response of macrophages towards co-infection with IAV and GAS was considerably distinct from the effects that were induced by either mono-infection. Although we encountered some similarities between the GAS and IAV+GAS groups, the preceding viral infection seemingly manipulated or obliterated the macrophages' reaction towards the bacterial pathogen by quantitative PCR and measured cytokine secretion by ELISA or bead-based multiplex analysis (Figure 4A). As illustrated in Figure 4B, the different (co-)infection regimens triggered distinct expression patterns of immunomodulatory agents that resulted in strong within-group associations, as shown via hierarchical clustering. IAV infection was specifically characterized by a relatively higher expression of *Mgl2* and

Tgfb1 (Figure 4C, Supplementary Figure S9). Bacterial infection, on the other hand, comprehensively stimulated the overexpression of several genes that mediate an inflammatory response (Figure 4B). Strikingly, co-infected macrophages mostly failed to induce a similar magnitude of GAS-inducible overexpression, yet upregulated *Arg1* (Figure 4B,C).

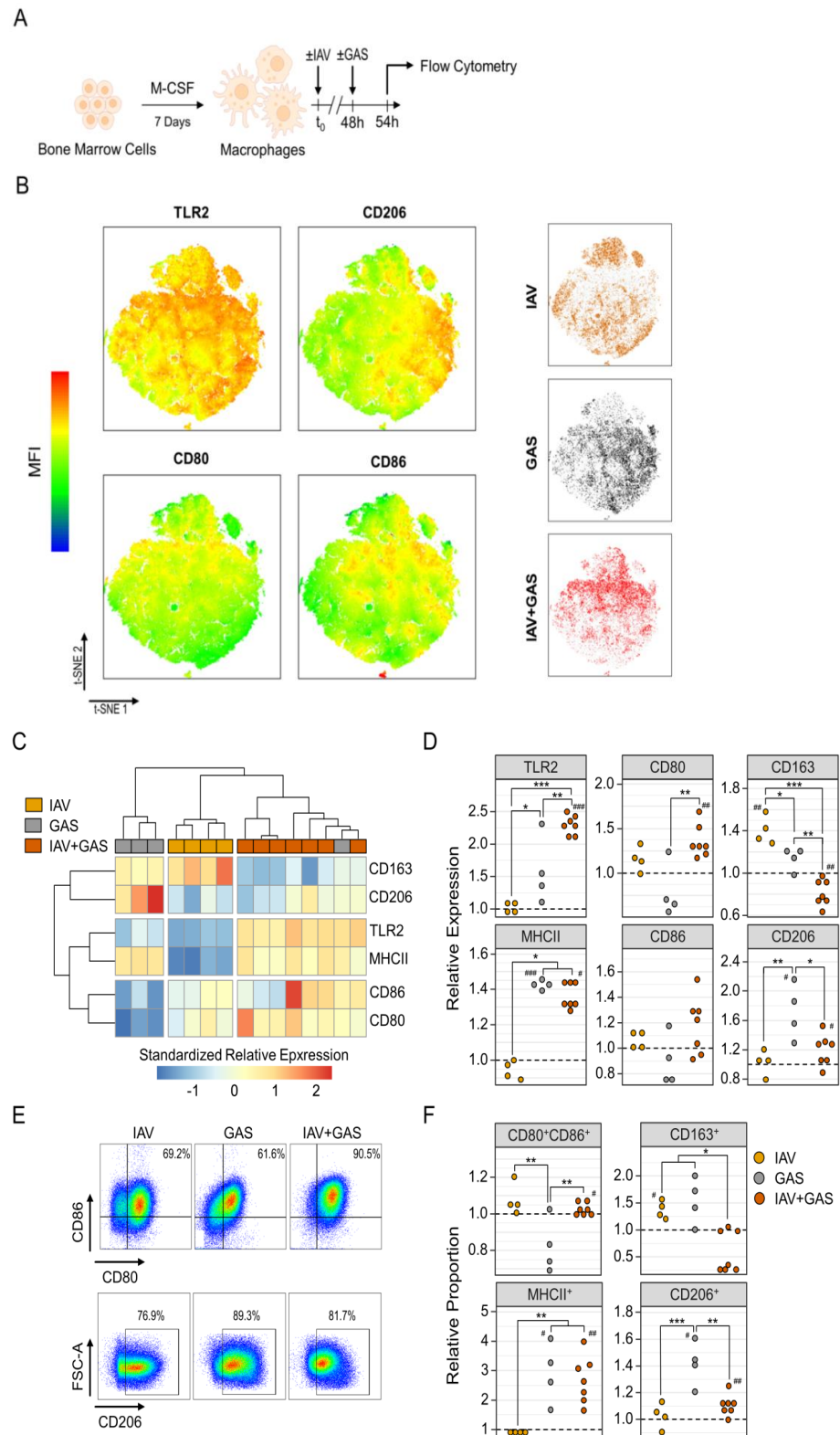


Figure 3. Activation of bone-marrow derived murine macrophages during in vitro co-infection was distinct from bacterial mono-infection. **(A)** Experimental Design. Macrophages were differentiated

from bone marrow cells and then infected with either IAV for 48 h (n = 4) or GAS for 6 h (n = 4). For co-infection, IAV was first applied for 48 h followed by GAS infection for 6 h (IAV+GAS, n = 7). Each sample was obtained from individual mice to obtain biological replicates. (B) t-distributed stochastic neighbor embedding (tSNE) on flow cytometry data from the three different macrophage infection models and topology of surface antigen expression levels. 10,000 events from each sample were integrated into the dimension reduction analysis. MFI: median fluorescence intensity. (C) Heatmap and hierarchical clustering on standardized fold changes of surface antigen expression levels based on their MFI. Fold changes were generated by normalization of MFI data from infected macrophages to their respective paired uninfected controls. (D) Dotplots depict the alteration of surface antigen expression levels due to (co-)infection. (E) Representative pseudocolor plots illustrate the alteration of proportions of macrophages expressing CD80 and CD86 (top) or CD206 (bottom) after (co-)infection. (F) Dotplots demonstrate the shift of macrophage subpopulation fractions after (co-)infection relative to uninfected controls (dashed lines). * $p < 0.05$, ** $p < 0.01$, *** $p < 0.001$, Dunn's test or Tukey HSD test with p -value adjustments for multiple comparisons (Bonferroni-Holm method). # $p < 0.05$, ## $p < 0.01$, ### $p < 0.001$, Wilcoxon signed-rank test or one-sample t -test for the comparison to uninfected cultures ($\mu = 1$).

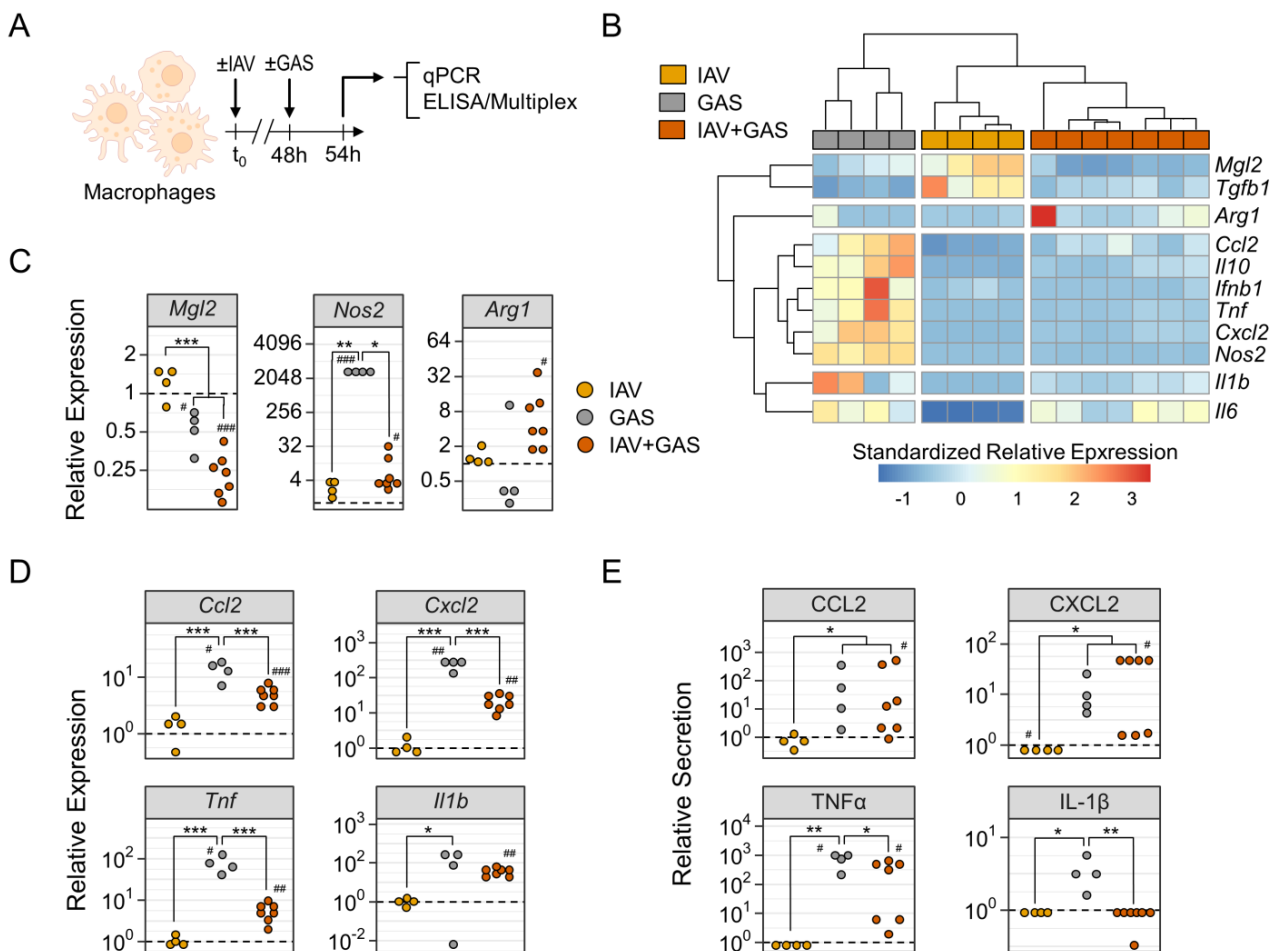


Figure 4. Preceding influenza A virus infection impedes pro-inflammatory immunological features of macrophages during co-infection. (A) Experimental Design. Bone-marrow derived macrophages were infected with IAV (n = 4), GAS (n = 4) or IAV+GAS (n = 7). Each sample was obtained from individual mice to obtain biological replicates. (B) Heatmap and hierarchical clustering on standardized relative mRNA expression levels from quantitative PCR analyses using the $2^{-\Delta\Delta Ct}$ method. Data from infected cultures were normalized to *Gapdh* and their respective paired uninfected controls. (C) Dotplots show the alterations of *Mgl2*, *Nos2* and *Arg1* mRNA expression levels due to (co-)infection. (D) Dotplots illustrate

distinct patterns of chemokine and cytokine mRNA production by macrophages after (co-)infection. (E) Dotplots demonstrate (co-)infection induced protein production of chemokines and cytokines that were measured in cell culture supernatants. Dashed lines represent control cultures. * $p < 0.05$, ** $p < 0.01$, *** $p < 0.001$, Dunn's test or Tukey HSD test with p -value adjustments for multiple comparisons (Bonferroni–Holm method). # $p < 0.05$, ## $p < 0.01$, ### $p < 0.001$, Wilcoxon signed-rank test or one-sample t -test for the comparison to uninfected cultures ($\mu = 1$).

By further examining individual expressions, we found that *Mgl2* was significantly reduced following bacterial mono-infection and co-infection by 1.8- and 3.9-fold, respectively, compared to uninfected controls (Figure 4C). Remarkably, GAS application induced an approximately 3000-fold overexpression of *Nos2* that was impeded during co-infection to a mere, yet statistically significant, 10-fold overexpression. Furthermore, co-infection triggered the upregulation of *Ccl2*, *Cxcl2* and *Tnf*, which were significantly less pronounced in comparison to GAS infection only (Figure 4D). Secretion of these cytokines was mostly comparable between these groups, however TNF α production by co-infected macrophages was reduced (Figure 4E). Although both *Il6* and *Il10* were increased in the GAS and IAV+GAS group, respectively, only co-infection caused a significant secretion of the protein products (Supplementary Figure S9). While *Ifnb1* was only upregulated following GAS infection, *Tgfb1* was downregulated after GAS infection as well as co-infection (Supplementary Figure S9A). Of note, although the GAS-induced overexpression of *Il1b* was also observed in the IAV+GAS group, co-infection entirely abrogated the secretion of mature IL-1 β , which suggests that a preceding IAV infection compromised innate immune sensing of Streptococci (Figure 4D,E).

In summary, the expression patterns of immunologically active mediators were noticeably different between GAS mono-infection and IAV+GAS co-infection, which implies that prior virus infection modifies anti-streptococcal immunity.

4. Discussion

In this study we demonstrated, for the first time, that influenza exacerbated subsequent intravenous GAS infection, which was indicated by an increased disease score as well as the elevated probability of paw edema occurrence. Although we did not assess any alterations in bone or cartilage morphology, we would like to argue that GAS induced paw swelling is reminiscent of septic arthritis [47]. Indeed, we previously demonstrated that the occurrence of paw edemas, which in the present study was more likely during IAV and GAS co-infection, was due to bacterial colonization of both subcutaneous and periarticular tissues and was paralleled by immune cell infiltration [35]. Hence, we show here for the first time that a preceding IAV infection predisposes the host to severe complications during GAS blood infection. Conversely, IAV infection elicited subsequent to intravenous GAS infection did not aggravate disease severity, which suggests that immune priming events in response to a prior viral encounter mitigate an otherwise competent anti-bacterial immune response.

Influenza in humans is usually characterized by mild-to-moderate disease that is rarely lethal and resolves shortly after infection [48], which was also shown in our animal model of IAV inoculation. Upon entry into nasopharyngeal cavities, the virus trespasses into the mucus, invades the epithelium and spreads to immune cells [49,50]. The host then recognizes parts of the viral RNA genome by intracellular pattern recognition receptors, which triggers the production of several inflammatory cytokines, among them type I IFNs, that establish an anti-viral immune state [51–53]. We have demonstrated that residual viral genes persisted for 16 days in the lungs of some infected mice, which was paralleled by a continuous upregulation of *Ifnb1*. However, we believe it to be unlikely that replicative viral particles were still present in the lungs up to this point because IAV is typically cleared within a couple days following infection and the quantities of viral genes were barely detectable in our samples [54–56]. Type I IFN can have beneficial effects during bacterial infection by promoting host resilience and by preventing systemic hyperinflammation [57–60]. However, several studies advocated that the consequences of

type I IFN expression are detrimental for the containment of a secondary bacterial insult subsequent to influenza [20,61,62].

By using a mouse strain that lacks the common IFN α/β receptor (IFNAR) in a model of pneumococcal superinfection, Shahangian et al. demonstrated that the IAV-induced IFNAR signaling led to an impaired production of the neutrophil attractants CXCL1 and CXCL2 [22]. They argued that, in agreement with a complementary study by Didierlaurent et al., type I IFNs desensitize subsequent TLR-mediated recognition of bacterial components by macrophages, which are major producers for these chemokines [22,23]. Another work on IFNAR^{-/-} mice by Nakamura and colleagues had some contrasting results concerning the impact of type I IFN signaling on pneumococcal superinfection [24]. In their study, they found that the virus and the bacteria were capable of synergistically inducing an overproduction of type I IFNs, which led to an impaired production of CCL2 while CXCL1/2 production was unaltered [24,63]. CCL2 supports bacterial clearance by the attraction of CCR2⁺ monocytes to the infected tissue [64,65]. Along these lines, we found in our study that CCL2 was significantly reduced in the plasma of IAV-infected mice and that both monocausal bacterial infection and co-infection featured *Ifnb1* overexpression in the lung. Hence, although the role of CCL2 during GAS infections is not yet fully elucidated, we find it possible that a preceding influenza restricts anti-bacterial immunity by limiting monocyte homing and their differentiation to macrophages not only in pulmonary tissues but also in remote host compartments that would be affected during GAS blood infection. However, the cellular source of this chemokine was not identified in our study and we were not able to confirm whether monocyte homing was indeed thwarted by IAV. Furthermore, the expression of *Ccl2* in lung samples that were taken at endpoints was comparable between bacterial infection and co-infection, which challenges the idea that IAV-induced alterations in immune cell recruitment continues after bacterial superinfection. In order to delineate the progression of co-infection in more detail, future studies should therefore focus on observations that are performed at specific time points rather than taking samples at endpoints that might be difficult to compare. For instance, in our study, only a small proportion of animals had genetic material from IAV in their lungs, which we assumed was due to the late time point at which IAV infection seemed to have resolved.

Apart from the ramifications due to an impaired chemokinesis, we suspected other means by which IAV dampens innate immune sensing of GAS. We hence focused on macrophage immunobiology in the context of co-infection and found that the virus comprehensively altered GAS-induced gene expression patterns and cytokine layout. In detail, we detected that the immune sensors CD163 and CD206 were markedly downregulated in co-infection compared to only GAS-infected macrophages. CD163 is an acute phase-regulated scavenger receptor that is exclusively expressed by cells of the monocyte lineage and aids in the removal of potentially toxic iron complexes during intravascular hemolysis [66–69]. Due to the fact that CD163 also mediates tissue repair [70], host resilience [66,68], immune resolution and is able to sense gram-positive bacteria [71,72], we speculate that this receptor might confer a protective immune state during hemolytic bacteremia, even though its role in GAS infection is yet underexplored. Similarly, the mannose receptor CD206 might support pathogen sensing during co-infection [73–77]; however, mice that lack this sensor molecule are not more susceptible to infection [78,79].

Strikingly, a preceding IAV inoculation notably reduced the GAS-induced upregulation of *Nos2* while boosting *Arg1* expression. Both genes code for enzymes that compete for the substrate L-Arginine, yet induce opposed immune mechanisms [80–82]. While nitric oxide synthase 2 (NOS2) provides inflammatory and bactericidal metabolites [83–85], arginase (ARG1) supports tissue repair and immune resolution [83]. Thus, our data hint at a distortion of anti-bacterial processes due to a prior IAV infection. This is further corroborated by an inadequate sensing of the bacterial pathogen indicated by the reduced and abolished production of TNF α and IL-1 β , respectively, which was similarly shown in a model of pneumococcal superinfection [19]. Interestingly, we detected an upregulation of *Il1b* for both GAS mono-infection and superinfection, which suggests that the incapacity

of co-infected macrophages to process and secrete IL-1 β is due to a failure in the GAS-inducible activation of the NLRP3 inflammasome [86–89]. In fact, it was shown that different variants of IAV, including a 2009 pandemic strain, were capable of thwarting IL-1 β maturation by interfering with NLRP3 inflammasome assembly [90–92], which is crucial for innate immune sensing and coordination [93]. An IAV-mediated nullification of IL-1 β secretion would be of dramatic consequences during streptococcal superinfections. The absence of signaling via the IL-1 receptor (IL-1R) was in fact associated with an increased susceptibility to systemic GAS infection in both mice and humans [86,94,95]. Remarkably, rheumatoid arthritis patients that received the IL-1R antagonist Anakinra exhibited a roughly 330-fold increased rate of invasive GAS infections which included an elevated likelihood of life-threatening complications such as necrotizing fasciitis and sepsis [95].

Although our study yielded several findings that are of interest to the research about influenza and bacterial co-infections, it has some limitations. Apart from the fact that our observations remained purely phenomenological and no experiments on underlying mechanisms were performed, we were unable to link the gap between our *in vivo* and *in vitro* models. For instance, we believe that the environment in which lung infection was combined with bacteremia was not suitably represented by using the method of macrophage co-infection described here. In detail, although we suspect that GAS was spreading to the lung, we did not show that the bacteria were in fact in contact with the same lung immune cells as the virus. Furthermore, the IAV-induced reduction of CCL2 in mice was not observed in macrophages that were challenged with the virus. Furthermore, it would have been interesting to test whether IAV impedes the capacity of macrophages to phagocytize GAS. Nevertheless, the multitude of IAV-inducible alterations to macrophage immunobiology in the context of GAS superinfection highlights the novelty of our study results and warrants further investigations.

In summary, we describe how IAV infection thwarts anti-streptococcal innate immunity in complementary *in vivo* and *in vitro* co-infection models. This finding warrants further investigations on the mechanisms underlying this phenomenon that sets the stage for post-influenza superinfection. As an important side issue, our work underscores the importance of regular vaccinations against influenza in order to avert bacterial superinfection and prevent fatal invasive GAS complications [10,96–100].

Supplementary Materials: The following supporting information can be downloaded at: <https://www.mdpi.com/article/10.3390/pathogens11111320/s1>, Figure S1: Gating Strategy for the analysis of murine bone marrow derived macrophages; Figure S2: PCR product lengths for influenza A virus genes; Figure S3: PCR product melting curves for influenza A virus genes; Figure S4: Eicosanoid production was not differentially regulated in paws from co-infected mice; Figure S5: PCR product lengths for Group A Streptococcus genes; Figure S6: PCR product melting curves for Group A Streptococcus genes; Figure S7: FlowSOM cluttering on flow cytometry data from infected macrophages; Figure S8: Surface antigen expression changes on macrophages after infection and co-infection; Figure S9: Expression and secretion of cytokines induced by infection or co-infection; Table S1: Primers for quantitative polymerase chain reaction of Influenza A genes; Table S2: Primers for quantitative polymerase chain reaction of Group A Streptococcus genes; Table S3: Pearson correlation analyses of sepsis scores with paw eicosanoids.

Author Contributions: J.A. and B.M.-H. designed the study. J.A., M.B., E.W., M.M., D.S., Ko-Infekt Study Group (K.M., M.L., U.B., A.S. and B.K.) designed and performed the experiments and collected the data. J.A., M.B. and D.S. performed the statistical analyses. J.A. wrote the first draft of the manuscript. All authors have read and agreed to the published version of the manuscript.

Funding: This research was funded by Federal Excellence Initiative of Mecklenburg-Western Pomerania and European Social Fund (ESF) Grant KoInfekt (ESF/14-BM-A55-0011/16 and ESF/14-BM-A55-0005/16). This study and J.A. were supported by a grant from the Deutsche Forschungsgemeinschaft (project VO 2697/2-1).

Data Availability Statement: The raw data supporting the conclusions of this article will be made available by the authors upon reasonable request.

Acknowledgments: The authors would like to thank Wendy Bergman for her excellent support during the work for this study. We also thank Dirk Koczan and Ildiko Toth for their help with the transcription analyses. Moreover, we like to express our gratitude to Karin Gerber and Chantal von Hörsten for their participation in the animal breeding and care at the animal core facility. The authors sincerely give their thanks to all staff and students that took part in the scientific discussions and experimental conduct.

Conflicts of Interest: The authors declare no conflict of interest.

References

1. Siemens, N.; Oehmcke-Hecht, S.; Mettenleiter, T.C.; Kreikemeyer, B.; Valentin-Weigand, P.; Hammerschmidt, S. Port d'Entrée for Respiratory Infections—Does the Influenza A Virus Pave the Way for Bacteria? *Front. Microbiol.* **2017**, *8*, 2602. [[CrossRef](#)] [[PubMed](#)]
2. Tjon-Kon-Fat, R.; Meerhoff, T.; Nikisins, S.; Pires, J.; Pereyaslov, D.; Gross, D.; Brown, C.; Drishti, A.; Hasibra, I.; Kota, M.; et al. The Potential Risks and Impact of the Start of the 2015–2016 Influenza Season in the WHO European Region: A Rapid Risk Assessment. *Influenza Other Respi. Viruses* **2016**, *10*, 236–246. [[CrossRef](#)] [[PubMed](#)]
3. McHardy, A.C.; Adams, B. The Role of Genomics in Tracking the Evolution of Influenza A Virus. *PLoS Pathog.* **2009**, *5*, e1000566. [[CrossRef](#)]
4. Neumann, G.; Noda, T.; Kawaoka, Y. Emergence and Pandemic Potential of Swine-Origin H1N1 Influenza Virus. *Nature* **2009**, *459*, 931–939. [[CrossRef](#)] [[PubMed](#)]
5. Taubenberger, J.K.; Morens, D.M. 1918 Influenza: The Mother of All Pandemics. *Emerg. Infect. Dis.* **2006**, *12*, 15–22. [[CrossRef](#)]
6. Morens, D.M.; Taubenberger, J.K.; Fauci, A.S. Predominant Role of Bacterial Pneumonia as a Cause of Death in Pandemic Influenza: Implications for Pandemic Influenza Preparedness. *J. Infect. Dis.* **2008**, *198*, 962–970. [[CrossRef](#)]
7. Brundage, J.F.; Shanks, G.D. Deaths from Bacterial Pneumonia during 1918–19 Influenza Pandemic. *Emerg. Infect. Dis.* **2008**, *14*, 1193–1199. [[CrossRef](#)]
8. Tasher, D.; Stein, M.; Simões, E.A.F.; Shohat, T.; Bromberg, M.; Somekh, E. Invasive Bacterial Infections in Relation to Influenza Outbreaks, 2006–2010. *Clin. Infect. Dis.* **2011**, *53*, 1199–1207. [[CrossRef](#)] [[PubMed](#)]
9. McKenna, S.; Malito, E.; Rouse, S.L.; Abate, F.; Bensi, G.; Chiarot, E.; Micoli, F.; Mancini, F.; Gomes Moriel, D.; Grandi, G.; et al. Structure, Dynamics and Immunogenicity of a Catalytically Inactive CXC Chemokine-Degrading Protease SpyCEP from *Streptococcus Pyogenes*. *Comput. Struct. Biotechnol. J.* **2020**, *18*, 650–660. [[CrossRef](#)]
10. Chaussee, M.S.; Sandbulte, H.R.; Schuneman, M.J.; DePaula, F.P.; Addengast, L.A.; Schlenker, E.H.; Huber, V.C. Inactivated and Live, Attenuated Influenza Vaccines Protect Mice against Influenza: *Streptococcus Pyogenes* Super-Infections. *Vaccine* **2011**, *29*, 3773–3781. [[CrossRef](#)]
11. Teymournejad, O.; Montgomery, C.P. Evasion of Immunological Memory by *S. Aureus* Infection: Implications for Vaccine Design. *Front. Immunol.* **2021**, *12*, 633672. [[CrossRef](#)] [[PubMed](#)]
12. Okamoto, S.; Kawabata, S.; Nakagawa, I.; Okuno, Y.; Goto, T.; Sano, K.; Hamada, S. Influenza A Virus-Infected Hosts Boost an Invasive Type of *Streptococcus Pyogenes* Infection in Mice. *J. Virol.* **2003**, *77*, 4104–4112. [[CrossRef](#)]
13. Okamoto, S.; Kawabata, S.; Terao, Y.; Fujitaka, H.; Okuno, Y.; Hamada, S. The *Streptococcus Pyogenes* Capsule Is Required for Adhesion of Bacteria to Virus-Infected Alveolar Epithelial Cells and Lethal Bacterial-Viral Superinfection. *Infect. Immun.* **2004**, *72*, 6068–6075. [[CrossRef](#)] [[PubMed](#)]
14. van der Sluijs, K.F.; Nijhuis, M.; Levels, J.H.M.; Florquin, S.; Mellor, A.L.; Jansen, H.M.; van der Poll, T.; Lutter, R. Influenza-Induced Expression of Indoleamine 2,3-Dioxygenase Enhances Interleukin-10 Production and Bacterial Outgrowth during Secondary Pneumococcal Pneumonia. *J. Infect. Dis.* **2006**, *193*, 214–222. [[CrossRef](#)] [[PubMed](#)]
15. Wang, B.; Li, S.; Southern, P.J.; Cleary, P.P. Streptococcal Modulation of Cellular Invasion via TGF- β 1 Signaling. *Proc. Natl. Acad. Sci. USA* **2006**, *103*, 2380–2385. [[CrossRef](#)]
16. Herrera, A.L.; Suso, K.; Allison, S.; Simon, A.; Schlenker, E.; Huber, V.C.; Chaussee, M.S. Binding Host Proteins to the M Protein Contributes to the Mortality Associated with Influenza–*Streptococcus Pyogenes* Superinfections. *Microbiology* **2017**, *163*, 1445–1456. [[CrossRef](#)]
17. Korteweg, C.; Gu, J. Pathology, Molecular Biology, and Pathogenesis of Avian Influenza A (H5N1) Infection in Humans. *Am. J. Pathol.* **2008**, *172*, 1155–1170. [[CrossRef](#)]
18. Plotkowski, M.C.; Bajolet-Laudinat, O.; Puchelle, E. Cellular and Molecular Mechanisms of Bacterial Adhesion to Respiratory Mucosa. *Eur. Respir. J.* **1993**, *6*, 903–916.
19. Sun, K.; Metzger, D.W. Inhibition of Pulmonary Antibacterial Defense by Interferon- γ during Recovery from Influenza Infection. *Nat. Med.* **2008**, *14*, 558–564. [[CrossRef](#)]
20. Navarini, A.A.; Recher, M.; Lang, K.S.; Georgiev, P.; Meury, S.; Bergthaler, A.; Flatz, L.; Bille, J.; Landmann, R.; Odermatt, B.; et al. Increased Susceptibility to Bacterial Superinfection as a Consequence of Innate Antiviral Responses. *Proc. Natl. Acad. Sci. USA* **2006**, *103*, 15535–15539. [[CrossRef](#)]
21. Metzger, D.W.; Sun, K. Immune Dysfunction and Bacterial Coinfections Following Influenza. *J. Immunol.* **2013**, *191*, 2047–2052. [[CrossRef](#)] [[PubMed](#)]

22. Shahangian, A.; Chow, E.K.; Tian, X.; Kang, J.R.; Ghaffari, A.; Liu, S.Y.; Belperio, J.A.; Cheng, G.; Deng, J.C. Type I IFNs Mediate Development of Postinfluenza Bacterial Pneumonia in Mice. *J. Clin. Investig.* **2009**, *119*, 1910–1920. [[CrossRef](#)] [[PubMed](#)]
23. Didierlaurent, A.; Goulding, J.; Patel, S.; Snelgrove, R.; Low, L.; Bebién, M.; Lawrence, T.; Van Rijt, L.S.; Lambrecht, B.N.; Sirard, J.C.; et al. Sustained Desensitization to Bacterial Toll-like Receptor Ligands after Resolution of Respiratory Influenza Infection. *J. Exp. Med.* **2008**, *205*, 323–329. [[CrossRef](#)] [[PubMed](#)]
24. Nakamura, S.; Davis, K.M.; Weiser, J.N. Synergistic Stimulation of Type I Interferons during Influenza Virus Coinfection Promotes Streptococcus Pneumoniae Colonization in Mice. *J. Clin. Investig.* **2011**, *121*, 3657–3665. [[CrossRef](#)]
25. Cunningham, M.W. Pathogenesis of Group A Streptococcal Infections. *Clin. Microbiol. Rev.* **2000**, *13*, 470–511. [[CrossRef](#)]
26. Musher, D. Trends in Bacteremic Infection Due to Streptococcus Pyogenes (Group A Streptococcus), 1986–1995. *Emerg. Infect. Dis.* **1996**, *2*, 54–56. [[CrossRef](#)]
27. Herrera, A.L.; Huber, V.C.; Chaussee, M.S. The Association between Invasive Group A Streptococcal Diseases and Viral Respiratory Tract Infections. *Front. Microbiol.* **2016**, *7*, 342. [[CrossRef](#)]
28. Jean, C.; Louie, J.K.; Glaser, C.A.; Harriman, K.; Hacker, J.K.; Aranki, F.; Bancroft, E.; Farley, S.; Ginsberg, M.; Hernandez, L.B.; et al. Invasive Group A Streptococcal Infection Concurrent with 2009 H1N1 Influenza. *Clin. Infect. Dis.* **2010**, *50*, 59–62. [[CrossRef](#)]
29. Zakikhany, K.; Degail, M.A.; Lamagni, T.; Waight, P.; Guy, R.; Zhao, H.; Efstratiou, A.; Pebody, R.; George, R.; Ramsay, M. Increase in Invasive Streptococcus Pyogenes and Streptococcus Pneumoniae Infections in England, December 2010 to January 2011. *Eurosurveillance* **2011**, *16*, 1–4. [[CrossRef](#)]
30. Okamoto, S.; Nagase, S. Pathogenic Mechanisms of Invasive Group A Streptococcus Infections by Influenza Virus–Group A Streptococcus Superinfection. *Microbiol. Immunol.* **2018**, *62*, 141–149. [[CrossRef](#)]
31. Goldmann, O.; Rohde, M.; Chhatwal, G.S.; Medina, E. Role of Macrophages in Host Resistance to Group A Streptococci. *Infect. Immun.* **2004**, *72*, 2956–2963. [[CrossRef](#)] [[PubMed](#)]
32. Ghoneim, H.E.; Thomas, P.G.; McCullers, J.A. Depletion of Alveolar Macrophages during Influenza Infection Facilitates Bacterial Superinfections. *J. Immunol.* **2013**, *191*, 1250–1259. [[CrossRef](#)] [[PubMed](#)]
33. Schultz, D.; Methling, K.; Rothe, M.; Lalk, M. Eicosanoid Profile of Influenza A Virus Infected Pigs. *Metabolites* **2019**, *9*, 130. [[CrossRef](#)] [[PubMed](#)]
34. Miller, M.A.; Stabenow, J.M.; Parvathareddy, J.; Wodowski, A.J.; Fabrizio, T.P.; Bina, X.R.; Zalduondo, L.; Bina, J.E. Visualization of Murine Intranasal Dosing Efficiency Using Luminescent Francisella Tularensis: Effect of Instillation Volume and Form of Anesthesia. *PLoS ONE* **2012**, *7*, e31359. [[CrossRef](#)]
35. Volzke, J.; Schultz, D.; Kordt, M.; Müller, M.; Bergmann, W.; Methling, K.; Kreikemeyer, B.; Müller-Hilke, B. Inflammatory Joint Disease Is a Risk Factor for Streptococcal Sepsis and Septic Arthritis in Mice. *Front. Immunol.* **2020**, *11*, 579475. [[CrossRef](#)]
36. Shrum, B.; Anantha, R.V.; Xu, S.X.; Donnelly, M.; Haeryfar, S.; McCormick, J.K.; Mele, T. A Robust Scoring System to Evaluate Sepsis Severity in an Animal Model. *BMC Res. Notes* **2014**, *7*, 233. [[CrossRef](#)]
37. Amend, S.R.; Valkenburg, K.C.; Pienta, K.J. Murine Hind Limb Long Bone Dissection and Bone Marrow Isolation. *J. Vis. Exp.* **2016**, *110*, 53936. [[CrossRef](#)]
38. Belkina, A.C.; Ciccolella, C.O.; Anno, R.; Halpert, R.; Spidlen, J.; Snyder-Cappione, J.E. Automated Optimized Parameters for T-Distributed Stochastic Neighbor Embedding Improve Visualization and Analysis of Large Datasets. *Nat. Commun.* **2019**, *10*, 5415. [[CrossRef](#)]
39. Van Gassen, S.; Callebaut, B.; Van Helden, M.J.; Lambrecht, B.N.; Demeester, P.; Dhaene, T.; Saeys, Y. FlowSOM: Using Self-Organizing Maps for Visualization and Interpretation of Cytometry Data. *Cytom. Part A* **2015**, *87*, 636–645. [[CrossRef](#)]
40. Gouwy, M.; Struyf, S.; Leutenez, L.; Pörtner, N.; Sozzani, S.; Van Damme, J. Chemokines and Other GPCR Ligands Synergize in Receptor-Mediated Migration of Monocyte-Derived Immature and Mature Dendritic Cells. *Immunobiology* **2014**, *219*, 218–229. [[CrossRef](#)]
41. Gomes, R.N.; Teixeira-Cunha, M.G.A.; Figueiredo, R.T.; Almeida, P.E.; Alves, S.C.; Bozza, P.T.; Bozza, F.A.; Bozza, M.T.; Zimmerman, G.A.; Castro-Faria-Neto, H.C. Bacterial Clearance in Septic Mice Is Modulated by MCP-1/CCL2 and Nitric Oxide. *Shock* **2013**, *39*, 63–69. [[CrossRef](#)] [[PubMed](#)]
42. Winter, C.; Taut, K.; Srivastava, M.; Länger, F.; Mack, M.; Briles, D.E.; Paton, J.C.; Maus, R.; Welte, T.; Gunn, M.D.; et al. Lung-Specific Overexpression of CC Chemokine Ligand (CCL) 2 Enhances the Host Defense to Streptococcus Pneumoniae Infection in Mice: Role of the CCL2-CCR2 Axis. *J. Immunol.* **2007**, *178*, 5828–5838. [[CrossRef](#)] [[PubMed](#)]
43. Valderrama, J.A.; Nizet, V. Group A Streptococcus Encounters with Host Macrophages. *Future Microbiol.* **2018**, *13*, 119–134. [[CrossRef](#)] [[PubMed](#)]
44. Carreno, D.; Wanford, J.J.; Jasiunaite, Z.; Hames, R.G.; Chung, W.Y.; Dennison, A.R.; Straatman, K.; Martinez-Pomares, L.; Pareek, M.; Orihuela, C.J.; et al. Splenic Macrophages as the Source of Bacteraemia during Pneumococcal Pneumonia. *EBioMedicine* **2021**, *72*, 103601. [[CrossRef](#)] [[PubMed](#)]
45. Ercoli, G.; Fernandes, V.E.; Chung, W.Y.; Wanford, J.J.; Thomson, S.; Bayliss, C.D.; Straatman, K.; Crocker, P.R.; Dennison, A.; Martinez-Pomares, L.; et al. Intracellular Replication of Streptococcus Pneumoniae inside Splenic Macrophages Serves as a Reservoir for Septicaemia. *Nat. Microbiol.* **2018**, *3*, 600–610. [[CrossRef](#)]
46. Horino, T.; Matsumoto, T.; Ishikawa, H.; Kimura, S.; Uramatsu, M.; Tanabe, M.; Tateda, K.; Miyazaki, S.; Aramaki, Y.; Iwakura, Y.; et al. Interleukin-1 Deficiency in Combination with Macrophage Depletion Increases Susceptibility to Pseudomonas Aeruginosa Bacteremia. *Microbiol. Immunol.* **2009**, *53*, 502–511. [[CrossRef](#)] [[PubMed](#)]

47. Newman, J.H. Review of Septic Arthritis throughout the Antibiotic Era. *Ann. Rheum. Dis.* **1976**, *35*, 198–205. [[CrossRef](#)]
48. Layne, S.P.; Beugelsdijk, T.J.; Patel, C.K.N.; Taubenberger, J.K.; Cox, N.J.; Gust, I.D.; Hay, A.J.; Tashiro, M.; Lavanchy, D. A Global Lab Against Influenza. *Science* **2001**, *293*, 1729. [[CrossRef](#)]
49. Manicassamy, B.; Manicassamy, S.; Belicha-Villanueva, A.; Pisanelli, G.; Pulendran, B.; Garcia-Sastre, A. Analysis of in Vivo Dynamics of Influenza Virus Infection in Mice Using a GFP Reporter Virus. *Proc. Natl. Acad. Sci. USA* **2010**, *107*, 11531–11536. [[CrossRef](#)]
50. Perrone, L.A.; Plowden, J.K.; Garcia-Sastre, A.; Katz, J.M.; Tumpey, T.M. H5N1 and 1918 Pandemic Influenza Virus Infection Results in Early and Excessive Infiltration of Macrophages and Neutrophils in the Lungs of Mice. *PLoS Pathog.* **2008**, *4*, e1000115. [[CrossRef](#)]
51. Iwasaki, A.; Pillai, P.S. Innate Immunity to Influenza Virus Infection. *Nat. Rev. Immunol.* **2014**, *14*, 315–328. [[CrossRef](#)] [[PubMed](#)]
52. Tough, D.F.; Borrow, P.; Sprent, J. Induction of Bystander T Cell Proliferation by Viruses and Type I Interferon in Vivo. *Science* **1996**, *272*, 1947–1950. [[CrossRef](#)] [[PubMed](#)]
53. Matikainen, S.; Pirhonen, J.; Miettinen, M.; Lehtonen, A.; Govenius-Vintola, C.; Sareneva, T.; Julkunen, I. Influenza A and Sendai Viruses Induce Differential Chemokine Gene Expression and Transcription Factor Activation in Human Macrophages. *Virology* **2000**, *276*, 138–147. [[CrossRef](#)] [[PubMed](#)]
54. Ip, D.K.M.; Lau, L.L.H.; Leung, N.H.L.; Fang, V.J.; Chan, K.-H.; Chu, D.K.W.; Leung, G.M.; Peiris, J.S.M.; Uyeki, T.M.; Cowling, B.J. Viral Shedding and Transmission Potential of Asymptomatic and Pauci-Symptomatic Influenza Virus Infections in the Community. *Clin. Infect. Dis.* **2016**, *64*, 736–742. [[CrossRef](#)]
55. Schwaiger, T.; Sehl, J.; Karte, C.; Schäfer, A.; Hühr, J.; Mettenleiter, T.C.; Schröder, C.; Köllner, B.; Ulrich, R.; Blohm, U. Experimental H1N1pdm09 Infection in Pigs Mimics Human Seasonal Influenza Infections. *PLoS ONE* **2019**, *14*, e0222943. [[CrossRef](#)]
56. Cuypers, F.; Schäfer, A.; Skorka, S.B.; Surabhi, S.; Tölken, L.A.; Paulikat, A.D.; Kohler, T.P.; Otto, S.A.; Mettenleiter, T.C.; Hammerschmidt, S.; et al. Innate Immune Responses at the Asymptomatic Stage of Influenza A Viral Infections of Streptococcus Pneumoniae Colonized and Non-Colonized Mice. *Sci. Rep.* **2021**, *11*, 20609. [[CrossRef](#)]
57. Kovarik, P.; Castiglia, V.; Ivin, M.; Ebner, F. Type I Interferons in Bacterial Infections: A Balancing Act. *Front. Immunol.* **2016**, *7*, 652. [[CrossRef](#)]
58. Castiglia, V.; Piersigilli, A.; Ebner, F.; Janos, M.; Goldmann, O.; Damböck, U.; Kröger, A.; Weiss, S.; Knapp, S.; Jamieson, A.M.; et al. Type I Interferon Signaling Prevents IL-1 β -Driven Lethal Systemic Hyperinflammation during Invasive Bacterial Infection of Soft Tissue. *Cell Host Microbe* **2016**, *19*, 375–387. [[CrossRef](#)]
59. LeMessurier, K.S.; Häcker, H.; Chi, L.; Tuomanen, E.; Redecke, V. Type I Interferon Protects against Pneumococcal Invasive Disease by Inhibiting Bacterial Transmigration across the Lung. *PLoS Pathog.* **2013**, *9*, e1003727. [[CrossRef](#)]
60. Maier, B.B.; Hladik, A.; Lakovits, K.; Korosec, A.; Martins, R.; Kral, J.B.; Mesteri, I.; Strobl, B.; Müller, M.; Kalinke, U.; et al. Type I Interferon Promotes Alveolar Epithelial Type II Cell Survival during Pulmonary Streptococcus Pneumoniae Infection and Sterile Lung Injury in Mice. *Eur. J. Immunol.* **2016**, *46*, 2175–2186. [[CrossRef](#)]
61. Antonelli, L.R.V.; Gigliotti Rothfuchs, A.; Gonçalves, R.; Roffê, E.; Cheever, A.W.; Bafica, A.; Salazar, A.M.; Feng, C.G.; Sher, A. Intranasal Poly-IC Treatment Exacerbates Tuberculosis in Mice through the Pulmonary Recruitment of a Pathogen-Permissive Monocyte/Macrophage Population. *J. Clin. Investig.* **2010**, *120*, 1674–1682. [[CrossRef](#)] [[PubMed](#)]
62. Jia, T.; Leiner, I.; Dorothee, G.; Brandl, K.; Pamer, E.G. MyD88 and Type I Interferon Receptor-Mediated Chemokine Induction and Monocyte Recruitment during *Listeria Monocytogenes* Infection. *J. Immunol.* **2009**, *183*, 1271–1278. [[CrossRef](#)] [[PubMed](#)]
63. Zimmerer, J.M.; Lesinski, G.B.; Radmacher, M.D.; Ruppert, A.; Carson, W.E. STAT1-Dependent and STAT1-Independent Gene Expression in Murine Immune Cells Following Stimulation with Interferon-Alpha. *Cancer Immunol. Immunother.* **2007**, *56*, 1845–1852. [[CrossRef](#)]
64. Zhang, Z.; Clarke, T.B.; Weiser, J.N. Cellular Effectors Mediating Th17-Dependent Clearance of Pneumococcal Colonization in Mice. *J. Clin. Investig.* **2009**, *119*, 1899–1909. [[CrossRef](#)] [[PubMed](#)]
65. Davis, K.M.; Nakamura, S.; Weiser, J.N. Nod2 Sensing of Lysozyme-Digested Peptidoglycan Promotes Macrophage Recruitment and Clearance of *S. Pneumoniae* Colonization in Mice. *J. Clin. Investig.* **2011**, *121*, 3666–3676. [[CrossRef](#)]
66. Kristiansen, M.; Graversen, J.H.; Jacobsen, C.; Sonne, O.; Hoffman, H.-J.; Law, S.K.A.; Moestrup, S.K. Identification of the Haemoglobin Scavenger Receptor. *Nature* **2001**, *409*, 198–201. [[CrossRef](#)]
67. Pulford, K.; Micklethwait, K.; McCarthy, S.; Cordell, J.; Jones, M.; Mason, D.Y. A Monocyte/Macrophage Antigen Recognized by the Four Antibodies GHI/61, Ber-MAC3, Ki-M8 and SM4. *Immunology* **1992**, *75*, 588–595.
68. Buechler, C.; Ritter, M.; Orsó, E.; Langmann, T.; Klucken, J.; Schmitz, G. Regulation of Scavenger Receptor CD163 Expression in Human Monocytes and Macrophages by Pro- and Antiinflammatory Stimuli. *J. Leukoc. Biol.* **2000**, *67*, 97–103. [[CrossRef](#)]
69. Oliviero, S.; Cortese, R. The Human Haptoglobin Gene Promoter: Interleukin-6-Responsive Elements Interact with a DNA-Binding Protein Induced by Interleukin-6. *EMBO J.* **1989**, *8*, 1145–1151. [[CrossRef](#)]
70. van den Heuvel, M.M.; Tensen, C.P.; van As, J.H.; van den Berg, T.K.; Fluitsma, D.M.; Dijkstra, C.D.; Döpp, E.A.; Droste, A.; van Gaalen, F.A.; Sorg, C.; et al. Regulation of CD163 on Human Macrophages: Cross-Linking of CD163 Induces Signaling and Activation. *J. Leukoc. Biol.* **1999**, *66*, 858–866. [[CrossRef](#)]
71. Fabrick, B.O.; van Bruggen, R.; Deng, D.M.; Ligtenberg, A.J.M.; Nazmi, K.; Schornagel, K.; Vloet, R.P.M.; Dijkstra, C.D.; van den Berg, T.K. The Macrophage Scavenger Receptor CD163 Functions as an Innate Immune Sensor for Bacteria. *Blood* **2009**, *113*, 887–892. [[CrossRef](#)] [[PubMed](#)]

72. Kneidl, J.; Löffler, B.; Erat, M.C.; Kalinka, J.; Peters, G.; Roth, J.; Barczyk, K. Soluble CD163 Promotes Recognition, Phagocytosis and Killing of Staphylococcus Aureus via Binding of Specific Fibronectin Peptides. *Cell. Microbiol.* **2012**, *14*, 914–936. [[CrossRef](#)] [[PubMed](#)]
73. Reading, P.C.; Miller, J.L.; Anders, E.M. Involvement of the Mannose Receptor in Infection of Macrophages by Influenza Virus. *J. Virol.* **2000**, *74*, 5190–5197. [[CrossRef](#)]
74. Pontow, S.E.; Kery, V.; Stahl, P.D. Mannose Receptor. *Int. Rev. Cytol.* **1993**, *137*, 221–244. [[CrossRef](#)]
75. Sallusto, F.; Cella, M.; Danieli, C.; Lanzavecchia, A. Dendritic Cells Use Macropinocytosis and the Mannose Receptor to Concentrate Macromolecules in the Major Histocompatibility Complex Class II Compartment: Downregulation by Cytokines and Bacterial Products. *J. Exp. Med.* **1995**, *182*, 389–400. [[CrossRef](#)] [[PubMed](#)]
76. Stahl, P.D. The Macrophage Mannose Receptor: Current Status. *Am. J. Respir. Cell Mol. Biol.* **1990**, *2*, 317–318. [[CrossRef](#)]
77. Upham, J.P.; Pickett, D.; Irimura, T.; Anders, E.M.; Reading, P.C. Macrophage Receptors for Influenza A Virus: Role of the Macrophage Galactose-Type Lectin and Mannose Receptor in Viral Entry. *J. Virol.* **2010**, *84*, 3730–3737. [[CrossRef](#)]
78. Lee, S.J.; Zheng, N.-Y.; Clavijo, M.; Nussenzweig, M.C. Normal Host Defense during Systemic Candidiasis in Mannose Receptor-Deficient Mice. *Infect. Immun.* **2003**, *71*, 437–445. [[CrossRef](#)]
79. Swain, S.D.; Lee, S.J.; Nussenzweig, M.C.; Harmsen, A.G. Absence of the Macrophage Mannose Receptor in Mice Does Not Increase Susceptibility to Pneumocystis Carinii Infection In Vivo. *Infect. Immun.* **2003**, *71*, 6213–6221. [[CrossRef](#)]
80. Gordon, S. Alternative Activation of Macrophages. *Nat. Rev. Immunol.* **2003**, *3*, 23–35. [[CrossRef](#)]
81. Wu, G.; Morris, S.M. Arginine Metabolism: Nitric Oxide and Beyond. *Biochem. J.* **1998**, *336*, 1–17. [[CrossRef](#)] [[PubMed](#)]
82. Starikova, E.A.; Sokolov, A.V.; Burova, L.A.; Golovin, A.S.; Lebedeva, A.M.; Vasilyev, V.B.; Freidlin, I.S. The Role of Arginine Deaminase from Streptococcus Pyogenes in Inhibition Macrophages Nitrogen Monooxide (NO) Synthesis. *Russ. J. Infect. Immun.* **2018**, *8*, 211–218. [[CrossRef](#)]
83. Hesse, M.; Modolell, M.; La Flamme, A.C.; Schito, M.; Fuentes, J.M.; Cheever, A.W.; Pearce, E.J.; Wynn, T.A. Differential Regulation of Nitric Oxide Synthase-2 and Arginase-1 by Type 1/Type 2 Cytokines In Vivo: Granulomatous Pathology Is Shaped by the Pattern of L-Arginine Metabolism. *J. Immunol.* **2001**, *167*, 6533–6544. [[CrossRef](#)]
84. Serbina, N.V.; Salazar-Mather, T.P.; Biron, C.A.; Kuziel, W.A.; Pamer, E.G. TNF/INOS-Producing Dendritic Cells Mediate Innate Immune Defense against Bacterial Infection. *Immunity* **2003**, *19*, 59–70. [[CrossRef](#)]
85. Tavares, L.P.; Teixeira, M.M.; Garcia, C.C. The Inflammatory Response Triggered by Influenza Virus: A Two Edged Sword. *Inflamm. Res.* **2017**, *66*, 283–302. [[CrossRef](#)] [[PubMed](#)]
86. Richter, J.; Brouwer, S.; Schroder, K.; Walker, M.J. Inflammasome Activation and IL-1 β Signalling in Group A Streptococcus Disease. *Cell. Microbiol.* **2021**, *23*, e13373. [[CrossRef](#)]
87. Harder, J.; Franchi, L.; Munoz-Planillo, R.; Park, J.-H.; Reimer, T.; Nunez, G. Activation of the Nlrp3 Inflammasome by Streptococcus Pyogenes Requires Streptolysin O and NF- κ B Activation but Proceeds Independently of TLR Signaling and P2X7 Receptor. *J. Immunol.* **2009**, *183*, 5823–5829. [[CrossRef](#)]
88. Lin, A.E.; Beasley, F.C.; Keller, N.; Hollands, A.; Urbano, R.; Troemel, E.R.; Hoffman, H.M.; Nizet, V. A Group a Streptococcus ADP-Ribosyltransferase Toxin Stimulates a Protective Interleukin 1beta-Dependent Macrophage Immune Response. *MBio* **2015**, *6*, e00133. [[CrossRef](#)]
89. Valderrama, J.A.; Riestra, A.M.; Gao, N.J.; LaRock, C.N.; Gupta, N.; Ali, S.R.; Hoffman, H.M.; Ghosh, P.; Nizet, V. Group A Streptococcal M Protein Activates the NLRP3 Inflammasome. *Nat. Microbiol.* **2017**, *2*, 1425–1434. [[CrossRef](#)]
90. Stasakova, J.; Ferko, B.; Kittel, C.; Sereinig, S.; Romanova, J.; Katinger, H.; Egorov, A. Influenza A Mutant Viruses with Altered NS1 Protein Function Provoke Caspase-1 Activation in Primary Human Macrophages, Resulting in Fast Apoptosis and Release of High Levels of Interleukins 1 β and 18. *J. Gen. Virol.* **2005**, *86*, 185–195. [[CrossRef](#)]
91. Park, H.S.; Lu, Y.; Pandey, K.; Liu, G.Q.; Zhou, Y. NLRP3 Inflammasome Activation Enhanced by TRIM25 Is Targeted by the NS1 Protein of 2009 Pandemic Influenza A Virus. *Front. Microbiol.* **2021**, *12*, 778950. [[CrossRef](#)] [[PubMed](#)]
92. Pothlichet, J.; Meunier, I.; Davis, B.K.; Ting, J.P.-Y.; Skamene, E.; von Messling, V.; Vidal, S.M. Type I IFN Triggers RIG-I/TLR3/NLRP3-Dependent Inflammasome Activation in Influenza A Virus Infected Cells. *PLoS Pathog.* **2013**, *9*, e1003256. [[CrossRef](#)] [[PubMed](#)]
93. Lamotte, L.A.; Tafforeau, L. How Influenza a Virus Ns1 Deals with the Ubiquitin System to Evade Innate Immunity. *Viruses* **2021**, *13*, 2309. [[CrossRef](#)]
94. Midiri, A.; Mancuso, G.; Beninati, C.; Gerace, E.; Biondo, C. The Relevance of Il-1-Signaling in the Protection against Gram-Positive Bacteria. *Pathogens* **2021**, *10*, 132. [[CrossRef](#)] [[PubMed](#)]
95. LaRock, C.N.; Todd, J.; LaRock, D.L.; Olson, J.; O'Donoghue, A.J.; Robertson, A.A.B.; Cooper, M.A.; Hoffman, H.M.; Nizet, V. IL-1 β Is an Innate Immune Sensor of Microbial Proteolysis. *Sci. Immunol.* **2016**, *1*, eaah3539. [[CrossRef](#)] [[PubMed](#)]
96. Ely, C.F. Influenza as Seen at the Puget Sound Navy Yard. *J. Am. Med. Assoc.* **1919**, *72*, 24. [[CrossRef](#)]
97. Okamoto, S.; Kawabata, S.; Fujitaka, H.; Uehira, T.; Okuno, Y.; Hamada, S. Vaccination with Formalin-Inactivated Influenza Vaccine Protects Mice against Lethal Influenza Streptococcus Pyogenes Superinfection. *Vaccine* **2004**, *22*, 2887–2893. [[CrossRef](#)]
98. Grabenstein, J.D. Immunization to Protect the US Armed Forces: Heritage, Current Practice, and Prospects. *Epidemiol. Rev.* **2006**, *28*, 3–26. [[CrossRef](#)]

-
99. Ozgur, S.K.; Beyazova, U.; Kemaloglu, Y.K.; Maral, I.; Sahin, F.; Camurdan, A.D.; Kizil, Y.; Dinc, E.; Tuzun, H. Effectiveness of Inactivated Influenza Vaccine for Prevention of Otitis Media in Children. *Pediatr. Infect. Dis. J.* **2006**, *25*, 401–404. [[CrossRef](#)]
 100. Clements, D.A. Influenza A Vaccine Decreases the Incidence of Otitis Media in 6- to 30-Month-Old Children in Day Care. *Arch. Pediatr. Adolesc. Med.* **1995**, *149*, 1113. [[CrossRef](#)]